International Journal of Nanomedicine

Dovepress
Taylor & Francis Group

Open Access Full Text Article

ORIGINAL RESEARCH

Emo@KP MBs Modulates the TGF-β1/Smad Signaling Pathway by in situ Micro-Nano Conversion to Reduce Renal Inflammation and Fibrosis Caused by Unilateral Ureteral Obstruction

Jinxia Zhang[1,2,*], Xinxin Xie[2,*], Yuanjing Li[1,*], Haonan Wang[2], Lijuan Zhang[1], Peiqi Shi[1], Jing Wei[1], Ling Zhang[1], Yingdong Lu[1], Ligang Cui[2], Xiaoning Liu[1], Xiaolong Liang[2]

[1]Department of Ultrasound, Guang'anmen Hospital, China Academy of Chinese Medical Sciences, Beijing, 100053, People's Republic of China; [2]Department of Ultrasound, Peking University Third Hospital, Beijing, 100191, People's Republic of China

*These authors contributed equally to this work

Correspondence: Xiaoning Liu; Xiaolong Liang, Email liuxn_angel2023@163.com; xiaolong_liang@bjmu.edu.cn

Introduction: Emodin alleviates renal interstitial fibrosis (RIF) and reduces inflammation by inhibiting the TGF-β1/Smad pathway, thus improving CKD outcomes. However, its clinical use is limited due to poor solubility and side effects. This study developed a targeted drug delivery system using αKIM-1 modified microbubbles carrying Emodin to enhance accumulation in renal tissues with high KIM-1 expression.

Methods: Emo@KP MBs were characterized by TEM and DLS, and their drug loading and encapsulation rates were measured by UV-VIS-NIR spectroscopy. Biocompatibility was assessed in vitro with HK-2 cells and in vivo via hematological and pathological markers. Contrast-enhanced ultrasound (CEUS) and fluorescence imaging were used for real-time visualization of treatment. Therapeutic experiments were performed on a unilateral ureteral obstruction (UUO) mouse model treated with Emo@KP MBs + US on days 1 and 3 post-surgery. Renal function, cytokine levels, and histological analysis were detected to evaluate therapeutic effects.

Results: Emo@KP MBs exhibited spherical structures (2 ~ 4 μm) with good stability. Ultrasound targeted microbubble destruction (UTMD) enabled controlled release of Emodin. CEUS and fluorescence imaging showed enhanced drug accumulation in diseased kidneys. In the UUO + Emo@KP MBs/US group, renal function was improved, inflammatory cytokines (IL-1β, TNF-α) were decreased, and renal lesions and collagen deposition were reduced. Immunohistochemistry revealed the downregulation of TGF-β, Smad2/3, and α-SMA, and upregulation of E-cadherin.

Conclusion: Emo@KP MBs enhanced drug delivery efficiency and therapeutic efficacy through αKIM-1 targeting and UTMD, while providing real-time imaging capabilities, suggesting good potential as a therapeutic approach to reduce renal inflammation and fibrosis in UUO.

Keywords: unilateral ureteral obstruction, renal interstitial fibrosis, microbubbles, UTMD, Emodin, αKIM-1

Introduction

The obstruction of ureter caused by stones or tumors is a common cause of hydronephrosis, which can eventually lead to the development of progressive chronic kidney disease (CKD) over time.[1–3] It has been found that progressive RIF and inflammation represent the primary pathological features of CKD. These are manifested by increased fibrin production, massive release of pro-inflammatory factors, and infiltration of inflammatory cells in the kidney.[4–7] The global prevalence

Received: 7 October 2024
Accepted: 4 March 2025
Published: 24 March 2025

of CKD is estimated to be 8 ~ 16%.[8] RIF is considered to be a common outcome of all CKD,[9] which is characterized by inflammation, myofibroblast activation and migration, extracellular matrix (ECM) deposition and remodeling. During the course of CKD, the fibrotic matrix is continuously deposited, causing the destruction of organ structure and the reduction of blood supply, which ultimately leads to organ dysfunction. Fibrosis of kidney tissue reduces its ability to self-repair, eventually leading to kidney failure.[10,11] As the incidence and mortality of CKD continue to rise year by year, it is clear that new strategies are urgently needed to prevent the development of CKD and improve the survival of patients. [12,13]

To better study treatment methods for CKD, UUO has been employed extensively to develop animal models of RIF, with ligation of the left ureter representing the most prevalent methodology.[2,14] The experimentally induced UUO model in rodents is believed to replicate the pathophysiology of human chronic obstructive kidney disease, facilitating the investigation of RIF mechanisms and the exploration of new drugs for the treatment of fibrosis.[2] The kidney after ureteral obstruction, undergoes a number of significant events, including mechanical stretching, activation of renin-angiotensin-aldosterone system, loss of renal epithelial cells, macrophage infiltration, inflammation, oxidative stress, and fibroblast activation. Collectively, these events lead to the eventual formation of RIF. Histologically, obstructive kidneys are characterized by the following features: tubular dilatation, interstitial dilatation, parenchymal loss, inflammatory cell infiltration, and ECM accumulation.[2,15] Infiltrated inflammatory cells produce and release a variety of profibrotic cytokines and growth factors, including transforming growth factor-β1 (TGF-β1), which activates both regulated (Smad-based) and non-regulated (non-Smad-based) signaling pathways, inducing interstitial fibroblast proliferation and myofibroblast transformation. This leads to excessive ECM deposition and RIF. Consequently, the targeted inhibition of the inflammatory response or TGF-β1/Smad signaling pathway may represent a potential therapeutic strategy for the inhibition of RIF.[16] Fortunately, the long history of traditional Chinese Medicine (TCM) in the treatment of RIF is well documented. TCM's multi-target and multi-link regulatory effects provide a promising avenue for the treatment of RIF. Emodin is an effective TCM for fibrotic diseases,[17] which has been demonstrated to effectively reduce the proliferation and metabolism of renal tubular epithelial cells, thereby alleviating the damage to the preserved nephron caused by high metabolism. Furthermore, it has been shown to effectively inhibit the proliferation and division of renal fibroblasts and promote their apoptosis, while it also reduced the infiltration of inflammatory cells within damaged kidneys. [18] Emodin has also been demonstrated to alleviate RIF by inhibiting TGF-β1 in UUO and doxorubicin-induced mouse models.[19,20] However, Emodin's application still has some shortcomings, which are mainly manifested as obvious toxic side effects.[21] Shukla et al reported that Emodin can induce cytotoxicity in primary rat hepatocytes by inhibiting the enzyme activity of NADPH quinone reductase.[22] Chen et al demonstrated that prolonged or high-dose Emodin administration can reduce glucuronidase activity and induce liver toxicity in humans and rats, suggesting a potential association between these variables.[23] In addition, Emodin has extremely poor water solubility, severely limiting its bioavailability. Therefore, there is an urgent need to develop an effective Emodin delivery system to improve the treatment of CKD.

Targeted drug delivery is crucial in disease treatment, and kidney injury molecule (KIM)-1, also known as T cell immunoglobulin mucin domain (TIM)-1, is an immunoglobulin superfamily protein that is significantly upregulated in the proximal tubules of the injured or diseased kidney. Its expression is observed early in the course of the disease, suggesting a role in the clearance of apoptotic cells.[24,25] The extracellular domain of KIM-1 is cleaved by matrix metalloproteinases and can be presented in rodent or human urine following proximal renal tubule injury. KIM-1 is expressed at a low level under normal physiological conditions, but following acute kidney injury, KIM-1 expression is significantly increased in the proximal tubule epithelial cells, which have undergone regeneration. The extracellular domain of KIM-1 molecules can be targeted to bind antibodies or drugs for imaging or therapy.[26,27] Herein, in light of the bottleneck problems associated with early diagnosis, monitoring, prevention and treatment of RIF, functional microbubbles consisted of phospholipid and sulfur hexafluoride were fabricated, with Emodin loading within the microbubble shell and KIM-1 antibody (αKIM-1) modifying on the surface, designated as Emo@KP MBs, for kidney diagnosis and treatment. With ultrasound imaging, the delivery of Emodin into the kidney can be clearly visualized. Then UTMD was applied to convert the MBs into NPs, the cavitation effect generated during this process increased the permeability of targeted tissues and facilitated the nanoparticles internalized into diseased tissues. The αKIM-1 further targeted the injured or diseased kidney, greatly enhanced the delivery efficiency of Emodin, which later reduced the inflammatory response by inhibiting the infiltration of inflammatory cells and the release of inflammatory factors, and alleviated the

process of RIF by inhibiting the TFG-β1/Smad signaling pathway. The biosafety of the prepared contrast agent was evaluated in vivo and in vitro, and the imaging and therapeutic properties of Emo@KP MBs were experimentally evaluated in UUO mouse models.

Materials and Methods

Experimental Animals

The experimental animals were SPF grade male Balb/c mice, 6 ~ 8 weeks old and weighing 18 ~ 20 g. The animals were purchased from the Laboratory Animal Center of Peking University Health Science Center and kept in SPF laboratory at a temperature of 18 ~ 22°C, humidity of 50 ~ 70%, and light cycle of 12 h. This experiment was approved by the experimental Animal Ethics Committee of Peking University Third Hospital (Ethics: LA2019206). In addition, the experiment followed the guidelines of the national standard GB/T 35892–2018 of the People's Republic of China Ethical Review Code for Experimental Animal Welfare.

Experiment Reagent

DSPC, DSPE-PEG_{2000} and DSPE-PEG_{2000}-NHS were purchased from Xi'an Ruixi Biotechnology Co., LTD. DSPE-PEG_{2000}-Cy5.5 was purchased from Shanghai Avito Biomedical Co., LTD. Emodin was purchased from Shanghai Aladdin Biochemical Technology Co., LTD. In Vivo MAb anti-mouse KIM-1 (αKIM-1) was purchased from Biox cell Biology. Mouse blood creatinine (CREA), blood urea nitrogen (UREA), glutamic-pyruvic transaminase (ALT) and glutamic-oxalacetic transaminase (AST) test kits were purchased from Jiancheng Bioengineering Research Institute, Nanjing. 3-(4,5)-dimethylthiahiazo (-z-y1)-3,5-di-phenytetrazoliumromide (MTT) and Calcein-AM/PI Live/Dead Viability/Cytotoxicity Assay kits were purchased from Beyotime Biotechnology Co., LTD. Mouse TNF-α ELISA kits and Mouse IL-1β ELISA kits were purchased from Solarbio Biotechnology Co., LTD. Other reagents of analytical purity can be purchased for direct use in experiments without further purification.

Experimental Method

Preparation and Optimization of Emo@KP MBs

Firstly, the optimal feeding ratio of αKIM-1 was investigated. Step 1: DSPC, DSPE-PEG_{2000} and DSPE-PEG_{2000}-NHS dissolved in ethanol were mixed evenly according to the molar ratio of 80:10:10 (total mass: 1 mg); Step 2: the lipid mixture was injected into 1 mL PBS in ultrasonic water bath; Step 3: Dialysis in PBS (interception molecular weight: 8000–14000 Da) for 1 day to remove organic solvent to obtain P NPs; Step 4: The suspension obtained by dialysis was reacted with αKIM-1 at room temperature in accordance with different mass ratios (20%, 30%, 40%, 50%, 60%), away from light; Step 5: Dialysis in PBS (molecular weight: 300000 Da) for 1 day to remove unlinked antibodies to obtain KP NPs; Step 6: Added KP NPs, propylene glycol and glycerol into 3 mL penicillin bottle according to the volume ratio of 80%:10%:10%, then filled with SF_6 gas, mechanical oscillation for 45 s, to obtain KP MBs. The optimal feeding ratio was determined by evaluating the connection rate of αKIM-1 and the size of the microbubbles.

Then, the optimal dosage ratio of Emodin was investigated as follows: Step 1: DSPC, DSPE-PEG_{2000} and DSPE-PEG_{2000}-NHS dissolved in ethanol were mixed evenly according to the molar ratio of 80:10:10 (total mass: 1 mg); Step 2: The lipid mixture was thoroughly mixed with Emodin according to different drug-lipid ratios (1/15, 1/10, 1/8, 1/5, 1/3); Step 3: The mixture of drugs and lipids was injected into 1 mL PBS under water bath ultrasound; Step 4: Dialysis in PBS (molecular weight: 8000–14000 Da) for 1 day to remove organic solvent and unencapsulated Emodin to obtain Emo@P NPs; Step 5: The suspension obtained by dialysis was reacted with the appropriate proportion of αKIM-1 obtained by the foregoing investigation at room temperature, away from light; Step 6: Dialysis in PBS (molecular weight: 300000 Da) for 1 day to remove unlinked antibodies to obtain Emo@KP NPs; Step 7: Emo@KP NPs, propylene glycol and glycerol were added into 3 mL penicillin bottle according to the volume ratio of 80%:10%:10%, then filled with SF_6 gas, Emo@KP MBs was obtained after mechanical oscillation for 45 s. The optimum feeding ratio of Emodin was determined by evaluating the encapsulation rate, loading rate and size of microbubbles.

For preparing Cy5.5-Emo@KP MBs, it is only necessary to substitute DSPE-PEG_{2000}-Cy5.5 for DSPE-PEG_{2000}.

Measurement of Size of Emo@KP MBs

The size of Emo@KP MBs was measured with a Coulter counter, and Emo@KP MBs were diluted with normal saline, and then the particle size was measured separately with normal saline after deducting the background. The average value of each sample was calculated by three parallel measurements.

Drug Loading Stability of Emo@KP MBs

Emodin is a lipophilic drug that is encapsulated in the shell layer of microbubbles by hydrophobic interaction. It gradually leaks and precipitates out of the microbubbles due to the higher concentration of Emodin in the microbubbles than in the solvent. In order to investigate the in vivo and in vitro drug-loading stability of Emo@KP MBs, the prepared microbubbles were stored at 37°C and 4°C. At the set time points (1, 2, 4, 8, 24 h), the microbubbles were centrifuged at 800 rpm/min for 5 min to separate the upper layer, which was then injected into organic reagents for detection of the Emodin content by Ultraviolet-Visible-Near-Infrared (UV-VIS-NIR) absorption spectroscopy. The content of Emodin in the microbubbles was quantified, and the leakage rate of the microbubbles was calculated based on the content of Emodin. The Emodin leakage rate was calculated as follows: 1 – (amount of Emodin within Emo@KP MBs/amount of drug initially loaded on Emo@KP MBs) × 100%.

Transmission Electron Microscopy Characterization of Emo@KP NPs

The optimized Emo@KP MBs were placed in a 24-well cell culture plate and subjected to UTMD (1.0 MHz, 10% duty cycle, 2.0 W/cm^2) for 30 s, and then the obtained Emo@KP NPs were added to the copper net by drops. After negative staining, they were air-dried and photographed under a transmission electron microscope (JEM-1400, Japan).

UV-VIS-NIR Absorption Spectrum Measurement

The absorption spectra of Emo@KP MBs and Emo@KP NPs were measured by UV-VIS-NIR spectrophotometer (UV2600, Shimadzu) with the wavelength range of 230 ~ 700 nm. Deionized water was used as baseline control, and free Emodin and αKIM-1 were used as drug controls.

Particle Size and Zeta Potential Measurement of Emo@KP NPs

The particle size and the Zeta potential of the Emo@KP NPs were measured three times using Malvern Zeta sizer Nano ZSP (UK) at 25°C.

The Ability of Contrast Enhanced Ultrasound (CEUS) of Emo@KP MBs in vitro

Emo@KP MBs were diluted with PBS to a concentration of 1 × 10^8 MBs/mL, and then 1 mL of ultrasonic microbubble contrast agent was taken and placed in a latex tube. The latex tube was placed in a crystallization dish filled with degassed water to measure the ultrasonic echo signals of the microbubbles at different time points.

Drug Release Under UTMD

An optimal drug delivery system should demonstrate stability within the blood circulation and facilitate the controlled release of the drug in response to internal or external stimuli upon reaching the targeted area. To investigate the drug release from Emo@KP MBs under exogenous ultrasound, we employed UTMD in vitro to blast Emo@KP MBs and subsequently monitored the release of Emodin. A 12-well plate was prepared, with 400 μL PBS added to each well. 100 μL Emo@KP MBs were then added to the PBS and mixed thoroughly. The plate was then subjected to ultrasound treatment, with the following parameters: 1.0 MHz, 2.0 W/ cm^2, 10% duty cycle, and ultrasound times of 0, 5, 30, and 120 s. After blasting, the liquid in the plate was collected and centrifuged at a low speed (800 rpm/min, 5 min). The lower layer of clarified liquid was then collected, and the Emodin content in the clarified liquid was detected by UV-VIS-NIR absorption spectrometry. This method allowed for the quantification of the drug released from Emo@KP MBs under the action of UTMD. The formula was as follows: Emodin release rate = (quantity of Emodin released from Emo@KP MBs/initial drug loaded on Emo@KP MBs) × 100%.

Selection and Culture of Cell Lines

We selected HK-2 cells as the model cell line and cultured them in complete DMEM/F12 medium in 5% CO_2 at 37°C. HK-2 cells were obtained from ATCC bank, which was a qualified repository that ensured the authenticity and quality of the cell lines, and their use was approved by Peking University Third Hospital.

Biocompatibility Assessment at the Cellular Level

Standard MTT assay and Live/Dead cell staining toxicity kit were used to evaluate the biocompatibility of Emo@KP MBs.

MTT experiment: HK-2 cells were seeded in 96-well plates at a density of 1×10^4 cells/well, after the cells were attached to the wall, the medium was replaced with medium containing different concentrations of Emo@KP MBs and cultured for another 24 h. Then, the medium was discarded, washed with PBS, and replaced with medium containing MTT (0.5 mg/mL) and continued to incubate for 4 h. Next, 200 μL DMSO was added and shaked for 15 min. The absorbance of 490 nm and 630 nm were measured by SPARK 10 M microplate reader, and the cell viability was calculated according to the absorbance.

$$\text{Cell Viability } (\%) = \frac{\text{OD}_{490\text{nm}}\text{Sample} - \text{OD}_{630\text{nm}}\text{Sample}}{\text{OD}_{490\text{nm}}\text{Blank} - \text{OD}_{630\text{nm}}\text{Blank}} \times 100\%$$

Live/Dead cells staining experiment: HK-2 cells were seeded in 24-well plates at a density of 2×10^5 cells/well, after the cells were attached to the wall, the medium was replaced with medium containing different concentrations of Emo@KP MBs and cultured for another 24 h. Then, the medium was discarded, and 500 μL pre-prepared Calcein-AM and Propyl iodide (PI) staining working solution was added and incubated for 30 min. Next, the working solution was discarded and washed with PBS 3 times. Finally, 500 μL PBS was added, then observed with a fluorescence microscope.

Biocompatibility Assessment at the Animal Level

The biosafety of Emo@KP MBs in vivo was evaluated by blood routine and blood biochemical analysis. The heart, liver, spleen, lung and kidney of mice injected with Emo@KP MBs were extracted, and pathological sections were taken to analyze whether pathological changes were caused.

Establishment of UUO Model

The mice were anesthetized by isoflurane inhalation at 0.8 ~ 1 L/min and intraperitoneal injection of tribromoethanol at a dose of 250 mg/kg. In the UUO group, ureteral ligation was performed on the left kidney near the renal hilus, and the ureteral ligation was performed a second time away from the renal hilus. In the Sham group, only the left ureter was freed without ligation, and the abdominal cavity was closed. After the surgical treatment, the mice were insulated and continued to be cultured in an SPF environment.

Administration in Model Mice

The UUO mice were randomly divided into the following 6 groups with 3 mice in each group: UUO + Control, UUO + US, UUO + Emo@P MBs, UUO + Emo@P MBs/US, UUO + Emo@KP MBs, UUO + Emo@KP MBs/US. Each group was administered microbubbles through the tail vein 1 and 3 days after UUO operation, respectively, and the group with ultrasound was irradiated immediately after administration. The mice were executed 10 days later for follow-up experiments.

Enzyme-Linked Immunosorbent Assay (ELISA)

When the mice were executed at the end of treatment, blood was taken from the mice's orbit veins. Then, related levels of factors including IL-1β and TNF-α in serum were detected according to the following protocols.

The samples to be tested and the standards of different concentrations were added to the microplate at 100 μL/well, covered with a sealing film, gently mixed, and incubated at room temperature for 2 h. After that, washed 3 times with 300 μL/well for 30 s each. Then, 100 μL HRP labeled IL-1β and TNF-α antibodies were added to each well, covered with a sealing film, and incubated at room temperature for 2 h. The washing steps described above were repeated, after which 100 μL chromogenic substrate was added to each well and incubated for 20 min at room temperature in the dark. Next,

50 μL of stop solution was added to each well, the color of the solution in the well changed from blue to yellow, and the absorbance value at 450 nm was measured by microplate reader within 30 min after adding the stop solution. 540 nm and 570 nm were used as the correction wavelengths. Corrected absorbance value = (OD_{450nm}-OD_{540nm}/OD_{570nm}). The concentrations of IL-1β and TNF-α in serum were calculated according to the standard curve.

Serum Levels of ALT, AST, CREA and UREA in Mice

ALT and AST catalyzed the amino-conversion of L-alanine, L-aspartic acid and α-ketoglutarate to pyruvate and oxaloacetate, respectively, and pyruvate and oxaloacetate converted NADH to NAD^+, which reduced the absorbance at 340 nm. UREA was hydrolyzed under the action of urease to form ammonia ions, which form a blue substance with phenol chromogenic agent in alkaline medium, which is proportional to the urea content, and has a characteristic absorption peak at 640 nm. CREA is hydrolyzed into glycine, formed aldehyde and H_2O_2 under the catalysis of creatinine amide hydrolase and creatine amino hydrolase, and H_2O_2 can be catalyzed with 2.4-DCP and 4-aminoantipyrine to form the purple-red compound quinonimines catalyzed by catalase, which has a characteristic absorption peak at 546 nm. Therefore, the absorbance values at 340 nm, 640 nm, and 546 nm were monitored and the contents of ALT, AST, CREA, and UREA were calculated by adding the corresponding substrate to the collected mouse serum.

Histological Analysis

After dissecting the diseased kidneys from each group, the kidneys were fixed with 4% paraformaldehyde, embedded in paraffin, and sliced at a thickness of 4 μm. HE staining and Masson staining were used to evaluate the pathological changes and the degree of renal fibrin deposition.

Immunohistochemistry Staining

The previously prepared kidney sections were dewaxed and rehydrated. Sections were treated with 0.3% H_2O_2 for 10 min, then antigens were extracted with 10% citrate buffer. The slices were incubated with primary antibody overnight at 4°C. After washing with PBS, incubated with secondary antibody for 30 min, and then incubated with DAB. Finally, hematoxylin was used for reverse staining and microscope imaging.

Statistical Analyses

All results were expressed as mean ± standard deviation. All statistical graphs were constructed using GraphPad Prism 10.0 software. One-way analysis of variance (ANOVA) was used to assess whether the differences between groups were statistically significant. $*\ P < 0.05,\ **\ P < 0.01,\ ***\ P < 0.001,\ ****\ P < 0.0001$ were considered statistically significant.

Results and Discussions

Fabrication and Characterization of Emo@KP MBs and US-Triggered in situ Micro-Nano Conversion

In order to obtain stable microbubbles for simultaneous delivery of Emodin and αKIM-1, the composition of the microbubbles must be carefully optimized. Emo@P NPs were first prepared from a lipid-drug mixture of DSPC, DSPE-PEG_{2000}, DSPE-PEG_{2000}-NHS and Emodin by the ethanol injection method under water bath sonication. αKIM-1 was then conjugated to Emo@P NPs via an amide reaction between the active NHS group of DSPE-PEG_{2000}-NHS and amino groups of αKIM-1 in PBS solution (pH 8.4). To obtain the appropriate ratio of αKIM-1 to P NPs, a series of weight ratios (w/w) of αKIM-1/P NPs (mAb/NPs) from 20% to 60% were designed to prepare KP NPs. The final binding efficiency and content of αKIM-1 conjugated to the P NPs surface were listed in Table S1 (Figure S1). With the increase of weight ratios (w/w) of mAb/P NPs, the amount of antibody connected to P NPs increased gradually from 14.37 ± 1.65% to 29.27 ± 0.85%. All these KP NPs were later mixed with propylene glycol and glycerol, filled with sulfur hexafluoride (SF_6), and mechanically oscillated to obtain the KP MBs (Figure 1). It can be observed that clear and transparent KP NPs (Figure S2A) became milky KP MBs (Figure S2B), which proved the successful preparation of microbubbles. In the process of mechanical oscillation, there was a high-frequency conversion between positive and negative pressures, which triggered the instability of the system, reduced the equilibrium concentration of

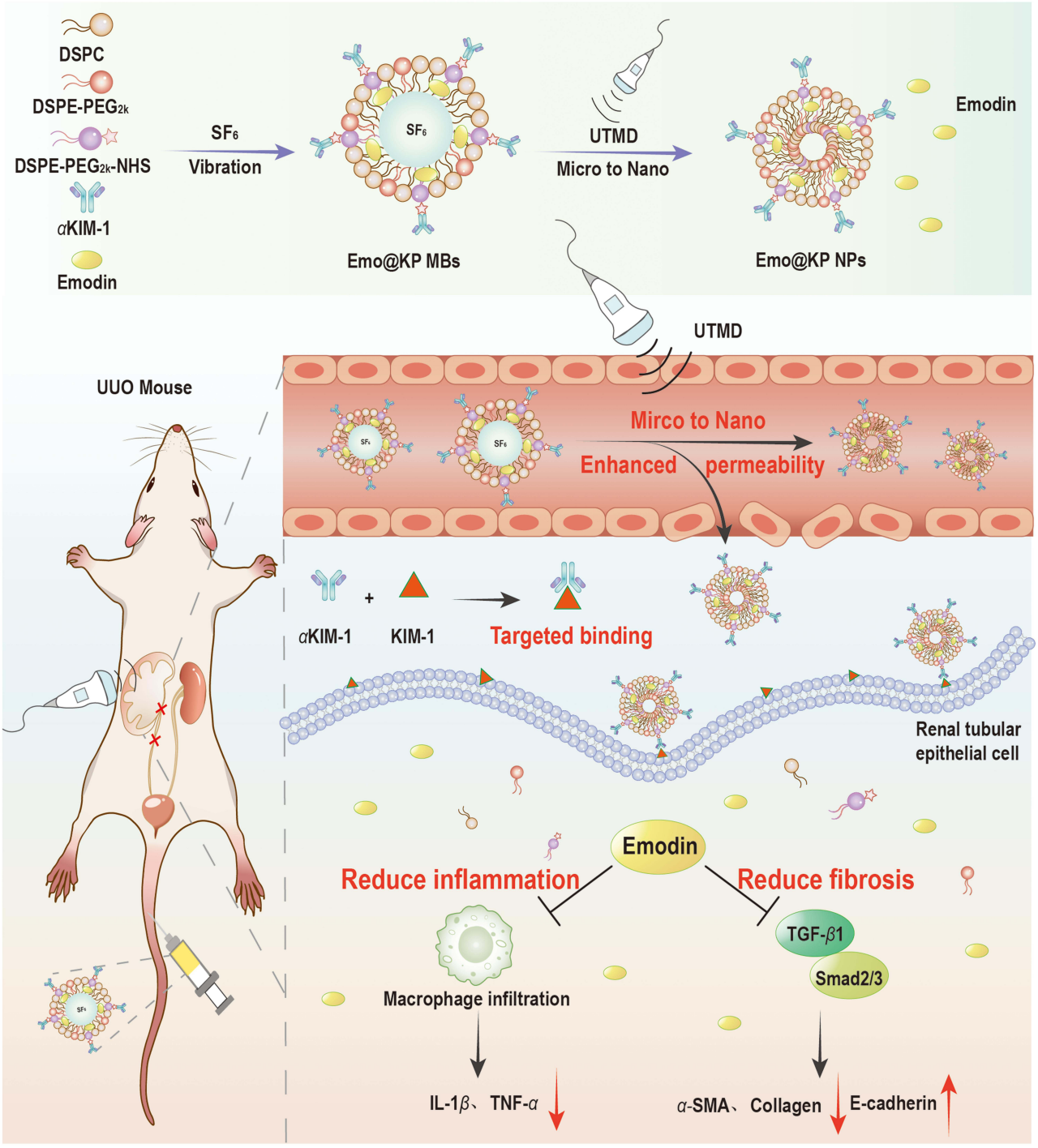

Figure 1 Illustration of the fabrication of Emo@KP MBs from emodin and αKIM-1, US mediated micro to nano conversion and mechanisms of Emo@KP MBs reducing renal inflammation and fibrosis.

SF_6 in KP NPs, decreased the solubility, and formed a large number of bubble nuclei in the matrix. These bubble nuclei gradually grew, formed tiny pores and eventually became microbubbles. Their size distribution was then investigated (Figure S3). However, considering the binding efficiency and content of αKIM-1, we selected 40% mAb/NPs for subsequent microbubble preparation.

Then, in order to obtain the appropriate ratio of Emodin to KP NPs, a series of Emo@KP NPs with the weight ratio (w/w) of Emodin/KP NPs (drug/lipids) ranging from 1/15 to 1/3 were designed. The encapsulation efficiency and loading

https://doi.org/10.2147/IJN.S499550

content of emodin were shown in Table S2 (Figure S4). With the increase of drug/lipids mass ratio (w/w), the encapsulation efficiency of Emodin firstly increased and then decreased, from 65.64% up to 82.94% and then down to 51.46%, but the loading content increased from 4.20% to 14.64%. All these Emo@KP NPs were transparent and orange, suggesting that the effective package of Emodin (Figure S5A), then Emo@KP NPs were mixed with glycerol and propylene glycol, filled with SF_6, mechanically oscillated to obtain opaque and orange Emo@KP MBs (Figure 1, Figure S5B), and size distribution was further measured (Figure S6). The results showed that when the mass ratio of drug/lipids (w/w) was less than 1/8, the size distribution of Emo@KP MBs was mainly ranged from 2 ~ 4 μm. As the drug/lipids ratio continued to increase, the particle size distribution of microbubbles became wider, and even a particle size of 10 μm appeared, which may cause vascular embolism if subsequently injected into the body. Therefore, after comprehensive consideration, the drug/lipids ratio of 1/8 was selected for the subsequent preparation of microbubbles.

Optical microscope images showed that Emo@KP MBs mostly had a spherical structure of 2 ~ 4 μm (Figure 2A), which was in good agreement with the size distribution measured by Coulter counter (Figure 2B). In order to investigate the morphological stability of Emo@KP MBs, it was stored in a refrigerator at 4°C and its size was monitored for 5 consecutive days (Figure 2C). The results showed that the size of Emo@KP MBs did not fluctuate significantly. Furthermore, the drug-loading stability of Emo@KP MBs was evaluated under simulated in vivo (37°C) and in vitro (4°C) conditions. At 4°C, drug release was observed to be (3.74 ± 0.11)% at 4 hours, (4.56 ± 0.32)% at 8 hours and (5.34 ± 0.37)% at 24 hours. At 37°C, the drug release exhibited a slight increase, reaching (4.78 ± 0.37)% at 4 hours, (6.37 ± 0.35)% at 8 hours and (7.67 ± 0.51)% at 24 hours, all of which remained within the acceptable limits. The aforementioned results indicated that the stability of Emo@KP MBs was good and well suited for its in vivo drug delivery (Figure 2D).

The absorption spectrum of Emo@KP MBs showed a characteristic absorption peak at ~430 nm, corresponding to the characteristic absorption peak of Emodin. The slight shift in this characteristic peak compared to Emodin should be due to the aggregation of these molecules during the self-assembly process. In addition, the UV−VIS-NIR absorption spectrum of Emo@KP MBs also changed at 280 nm, which was attributed to the absorption peak of the conjugated double bonds of tryptophan residues and tyrosine residues in αKIM-1 (Figure 2E). Besides, the presence of αKIM-1 in the microbubbles was observed under fluorescence microscopy through the labeled fluorescent secondary antibodies. These results indicated that Emodin and αKIM-1 successfully loaded onto Emo@KP NPs (Figure 2F).

To explore whether Emo@KP MBs could be converted into Emo@KP NPs, they were exposed to US (1 MHz, 10% duty cycle, 2 W/cm^2) for 30 s. TEM images showed that Emo@KP NPs had a size of ~70 nm (Figure 2G), which was smaller than the hydrodynamic light scattering measurements (~110 nm) due to the lack of hydration layer (Figure 2H). These results confirmed that Emo@KP MBs can be efficiently converted to Emo@KP NPs after exposure to US, further promoting the in vivo transformation of MBs into NPs in diseased tissues. We monitored the surface charge of Emo@KP NPs, and the results showed that it was −25.4 ± 0.32 mV, which allowed it to circulate in the blood for a long time and avoided being cleared by the liver and spleen (Figure S7).

Emo@KP MBs were diluted with saline, and its imaging capability was observed under a clinical ultrasound system. The experimental results showed that the targeted microbubbles presented uniform and dense point-like strong echoes under the ultrasonic enhancement mode, which proved that the targeted microbubbles had good ultrasonic imaging effect. Subsequently, US was used to blast the microbubbles, and its imaging ability was lost, further indicated that the microbubbles were destroyed and formed nanoparticles (Figure 2I). Then, we evaluated the CEUS enhancement time of Emo@KP MBs. The results showed that the echo signal of Emo@KP MBs can still be observed after 20 min (Figure 2J). Therefore, Emo@KP MBs offered the possibility of visualizing therapy in real time with an adequate time window.

Drug Release of Emo@KP MBs in Response to UTMD

Previous studies[28] have shown that the conditions for typical sonoporation and acoustic cavitation effects were 37°C, 1.0 MHz, 2.0 W/cm^2, 10% duty cycle, 0 ~ 2 min exposure time. Under the action of UTMD, the microbubbles blasted to release the drug encapsulated in the shell. For microbubbles with different particle sizes, the exposure time for optimal micro-nano conversion by ultrasonic bursting is different. Therefore, the exposure time was screened for optimal drug

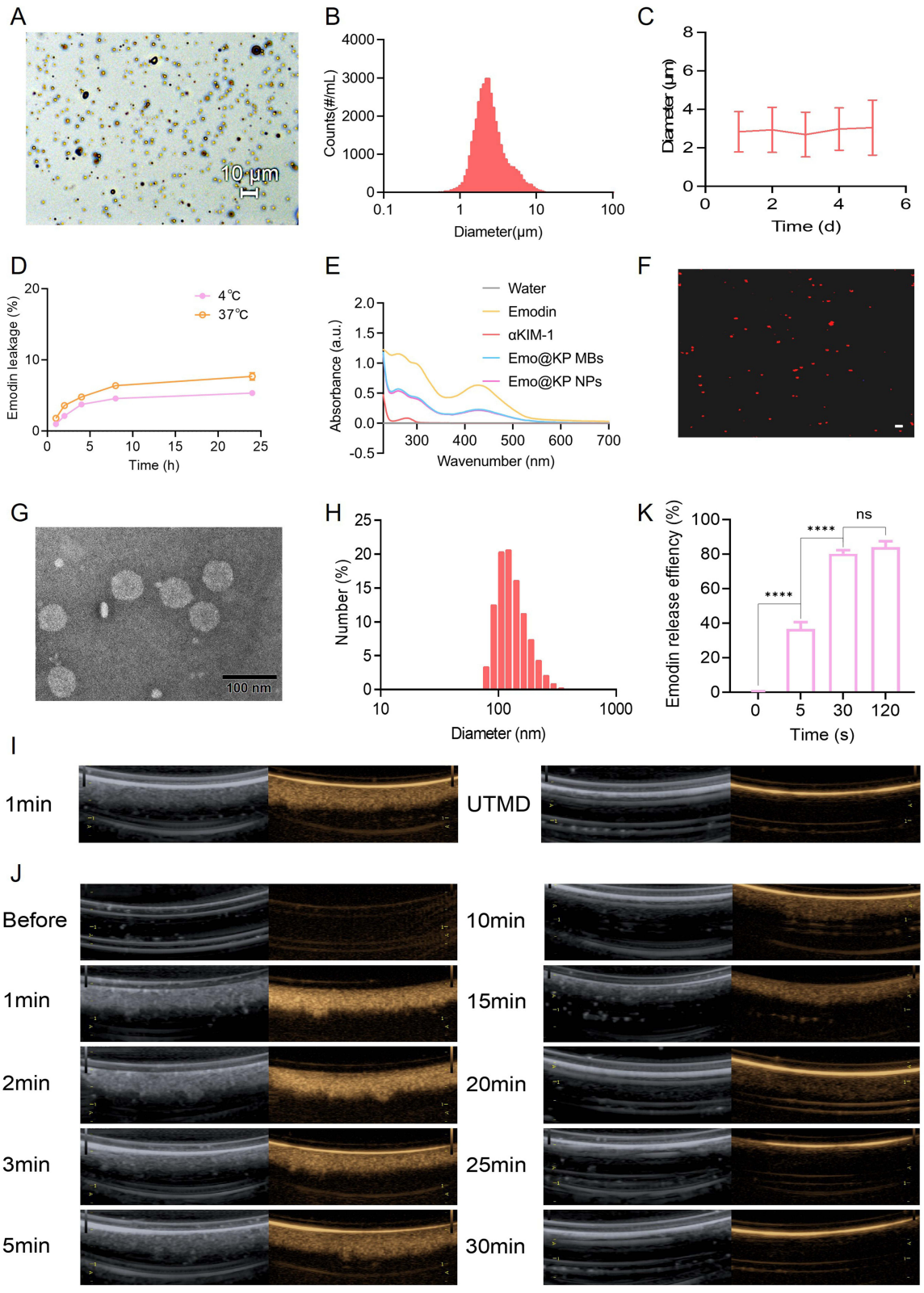

Figure 2 Characterization of Emo@KP MBs and US-triggered in situ micro-to-nano conversion. (**A**) Light microscopy image of Emo@KP MBs. Scale bar:10 μm; (**B**) Size distribution of Emo@KP MBs; (**C**) Particle size stability of Emo@KP MBs; (**D**) Drug loading stability of Emo@KP MBs; (**E**) UV–VIS-NIR absorption spectra of Emodin, αKIM -1, Emo@KP MBs and Emo@KP NPs; (**F**) Fluorescence images of Emo@KP MBs, where red fluorescence represented the αKIM-1. Scale bar:10 μm; (**G**) TEM image of Emo@KP NPs converted from Emo@KP MBs upon US exposure (1MHz, 10% duty cycle, 2W/cm^2, 30 s). Scale bar: 100 nm; (**H**) Hydrodynamic size distribution of Emo@KP NPs; (**I**) The destruction of Emo@KP MBs was confirmed by contrast-enhanced ultrasound in vitro; (**J**) US imaging of Emo@KP MBs at different times in vitro; (**K**) Emodin release efficiency under different ultrasound exposure time (**** $P < 0.0001$).

https://doi.org/10.2147/IJN.S499550

release. The results were presented in Figure 2K. In the absence of the UTMD effect, Emo@KP MBs exhibited only (0.43 ± 0.1)% drug release during the experiment. When the exposure time was increased from 5 to 30 s, the Emodin release rate was increased from (36.63 ± 4.0)% to (80.23 ± 2.06)%. However, with an increase in exposure time up to 120 seconds, the Emodin release rate was observed to be (84.05 ± 3.43)% and did not demonstrate a significant increase. The reason may be that under typical sonoporation and acoustic cavitation conditions, 30 s of ultrasonic time blasted most of the microbubbles and released more than 80% of the encapsulated drug. The above results demonstrated that UTMD can promote the conversion of microbubbles to nanoparticles, the energy generated in the process disintegrated the nanoparticles, released Emodin contained in them, thus realizing the controlled drug release, and the most cost-effective ultrasonic irradiation time was 30 s.

Biosafety Assessment

Good biocompatibility is a prerequisite for the use of micro/nano drugs in vivo. Firstly, the biocompatibility was evaluated at the cellular level by incubating Emo@KP MBs with HK-2 cells at different concentrations for 24 h. Then, standard MTT assay and Live/Dead cell staining were applied. The results showed that high concentration of Emo@KP MBs (200 μg/mL) had no significant influence, and the cell survival rate was above 90% (Figure 3A and B). The results of Live/Dead cell staining showed strong green fluorescence signals and almost no red fluorescence signal, which further indicated that the use of antibody linked microbubbles as drug delivery carriers had good biocompatibility.

Then, the biosafety of Emo@KP MBs was evaluated by blood routine, blood biochemical test and histological analysis. Emo@KP MBs (200 μL, equivalent Emodin concentration: 10 mg/kg) was injected into mice through the tail vein, then peripheral blood routine examination was performed before injection (Control) and 1, 2, 3, and 5 days after injection. There were no significant changes in all key blood parameters after injection of Emo@KP MBs, indicating that Emo@KP MBs did not cause adverse infection or inflammation (Figure 3C–J). The main blood biochemical indexes of the mice did not change significantly, which can also prove the above conclusion (Figure 3K–N). On the 10th day, the mice were euthanized, and the major organs were removed for histopathological analysis, no significant pathological damage was found at the histological level (Figure 3O). Therefore, the results of in vitro and in vivo experiments indicated that Emo@KP MBs had lower systemic toxicity and better biosafety.

Successful Construction of Balb/c Mouse' UUO Model

UUO is a model of RIF whereby the ureter is ligated unilaterally, resulting in urinary tract obstruction, reduced renal blood perfusion, macrophage infiltration, fibrocyte proliferation, and scar formation. It mainly causes fibrosis and atrophy of renal tubules and has little impact on glomeruli, without symptoms such as hypertension, proteinuria and abnormal lipid metabolism. The UUO model mice exhibit a rapid progression of RIF, with related features appearing as early as 7 days postoperatively. RIF is characterized by the deposition of matrix proteins between the tubular basement membrane and the peritubular capillaries, which enlarges the distance between them. In physiological conditions, renal tubular interstitial collagen synthesis and degradation are precisely regulated. In contrast, in RIF, activated myofibroblasts produce excess collagen, which causes a sparse distribution of peritubular capillaries and leads to hypoxia in renal tubular epithelial cells. Hypoxia in renal tubular epithelial cells upregulates pro-fibrotic pathways, thus creating a cycle that exacerbates renal fibrosis.

To validate the successful construction of the model, we evaluated the kidneys of post-UUO versus post-Sham mice in pathological sections and used the kidneys of healthy mice without surgery as controls. Compared with the kidneys of the Sham group and the unobstructed contralateral group, the kidneys on the operated side of the UUO mice gradually showed tubulointerstitial damage on the first day after surgery, which was manifested by tubular dilatation, epithelial detachment, basement membrane thickening and increased infiltration of inflammatory cells in the interstitial space on HE staining. The manifestation became more and more pronounced with prolonged post-operative time, and obvious renal fibrosis and cortical atrophy appeared on the 7th day after the operation. In contrast, the renal tubules on the contralateral side of the surgical kidneys in the UUO group and Sham group were neatly aligned and regular in morphology, with no inflammatory cell infiltration (Figure 4A, C, D, E).

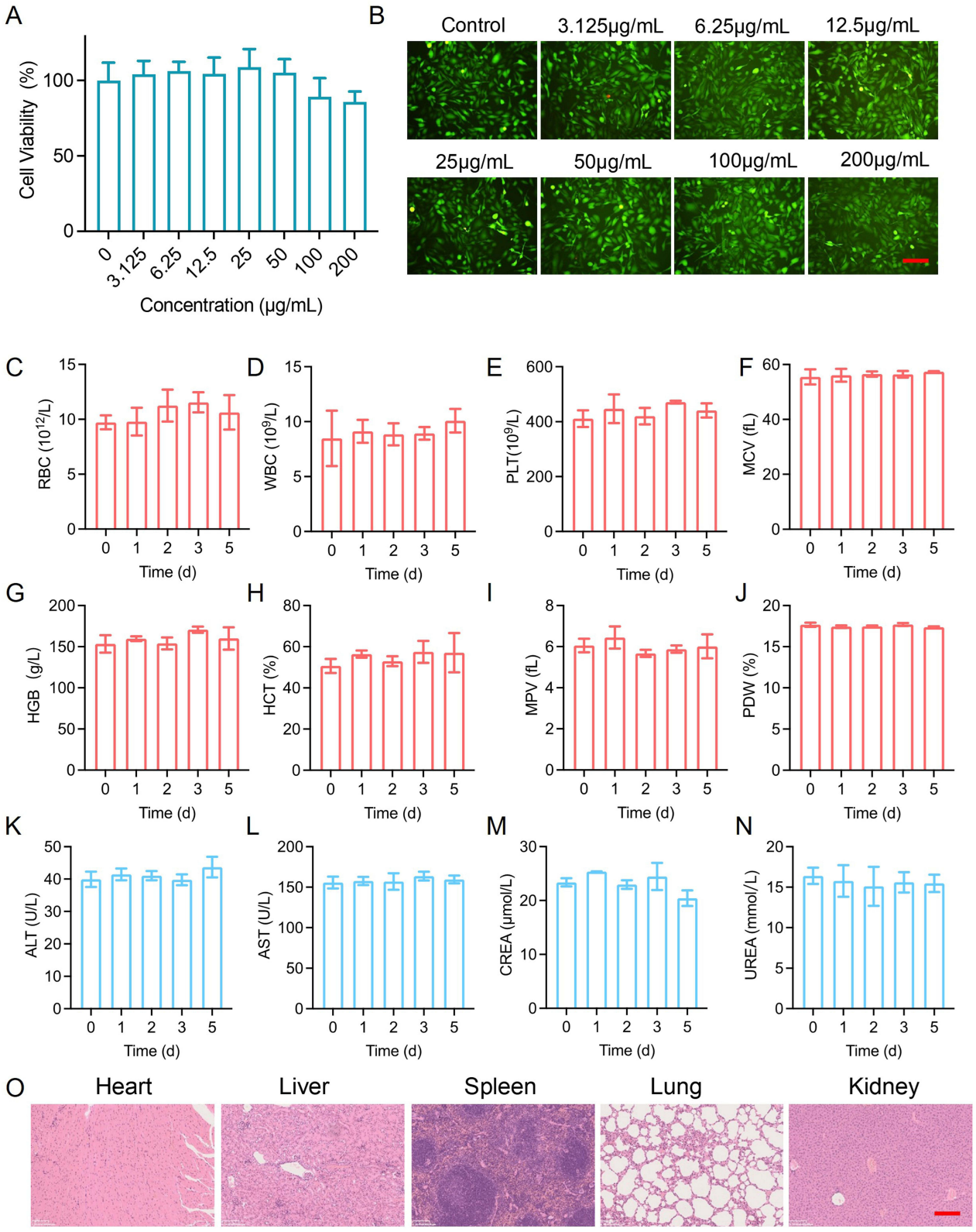

Figure 3 Biosafety assessment. (**A**) Viability of HK-2 cells incubated with different concentrations of Emo@KP MBs for 24 h; (**B**) Fluorescence images of HK-2 cells stained with Live/Dead activity/toxicity kit after treated with different concentrations of Emo@KP MBs. Scale bar: 100 μm; (**C–J**) Primary indicators of blood routine tests of mice at days 1, 2, 3, and 5 after injection of Emo@KP MBs; (**K–N**) Primary indicators of blood biochemical results of mice at days 1, 2, 3, and 5 after injection of Emo@KP MBs; (**O**) HE staining of mice at day 14 after injection of Emo@KP MBs. Scale bar: 100 μm.

https://doi.org/10.2147/IJN.S499550

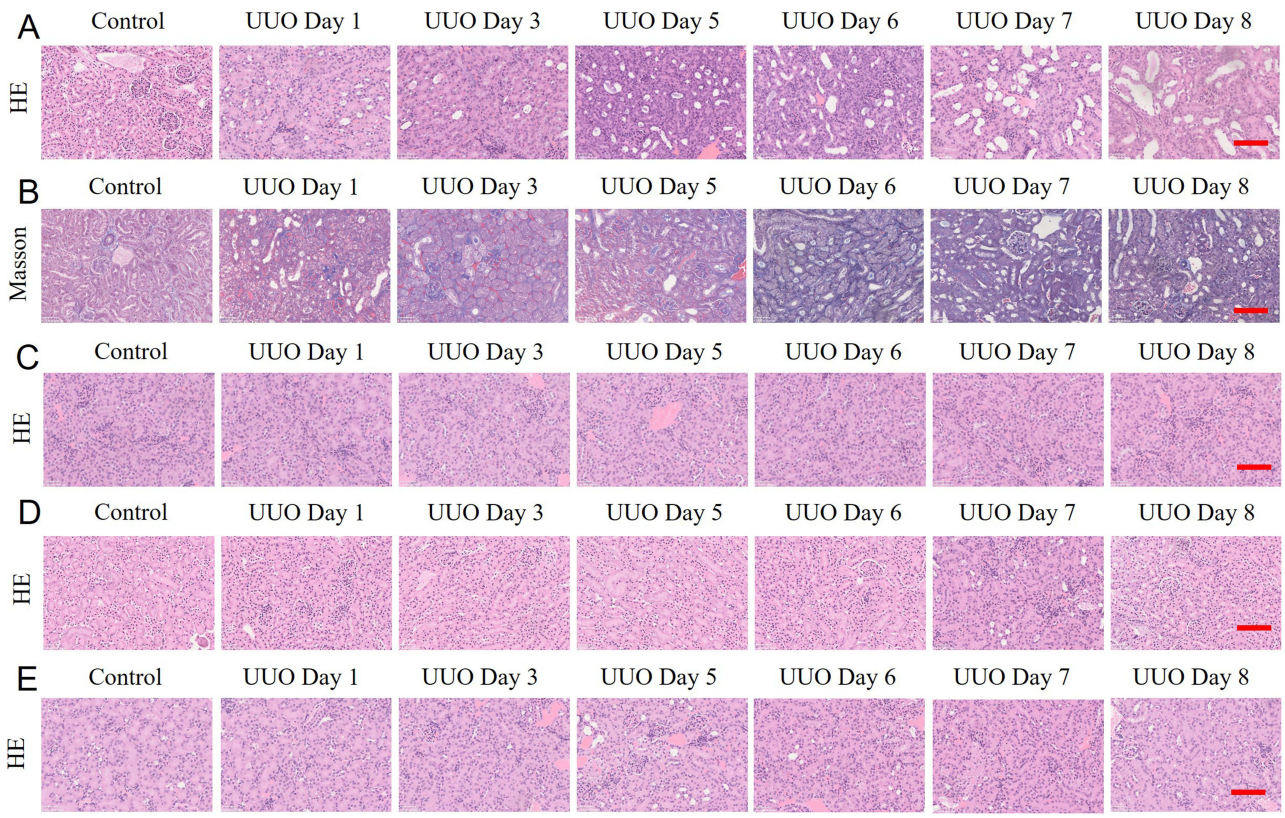

Figure 4 Pathological changes of bilateral kidney after UUO and Sham operation were analyzed, healthy mouse's kidneys were used as controls for all results. (**A**) HE staining of kidney sections from the operated side of mice after UUO surgery; (**B**) Masson staining of kidney sections from the operated side of mice after UUO surgery; (**C**) HE staining of kidney sections from the non-operated side of mice after UUO surgery; (**D**) HE staining of kidney sections from the operated side of mice after Sham surgery; (**E**) HE staining of kidney sections from the non-operated side of mice after Sham surgery. Scale bar: 100 μm.

Masson staining is the most classic method of connective tissue staining. On Masson staining, muscle fibers appear red and collagen fibers appear green or blue. It is mainly used to distinguish collagen fibers from muscle fibers. In comparison to the Sham group and contralateral side of the surgical kidneys following UUO, the diseased kidneys in the UUO group exhibited a considerable number of renal tubular epithelial cells atrophied, tubular lumen dilated, and a substantial number of blue collagen fibers observed in the interstitium on Masson staining. Moreover, a small amount of blue collagen fiber staining appeared on the first day after surgery in the interstitial tissues of the kidney. With the extension of postoperative time, collagen deposition in the renal interstitial tissue increased, and the blue color became more obvious (Figure 4B).

These findings indicated that we have successfully constructed a mouse model of RIF and provided a basis for the timing of subsequent treatment experiments.

US Imaging and Biodistribution Assessment

The ability of Emo@KP MBs to enhance ultrasound imaging in vivo was evaluated using a clinical ultrasound system (VINNO70). As shown in Figure 5A, no echo signal was observed on the diseased kidney before the injection of Emo@KP MBs, but obvious CEUS signal could be observed on the diseased kidney 10 s after the injection of Emo@KP MBs, indicating that targeted microbubbles flowed in kidney blood vessels and enhanced CEUS imaging could be achieved. And the contrast signal was still very obvious until 5 min after the injection. In addition, the prepared Emo@KP MBs can clearly indicate the viable site of the diseased kidney, which had better diagnostic effect than two-dimensional ultrasound.

Cy5.5-Emo@KP MBs were prepared using the Cy5.5 labeling of Emo@KP MBs (Figure S8). The fluorescence of Cy5.5 on Emo@KP MBs was detected by fluorescence imaging to further monitor the drug enrichment in the diseased

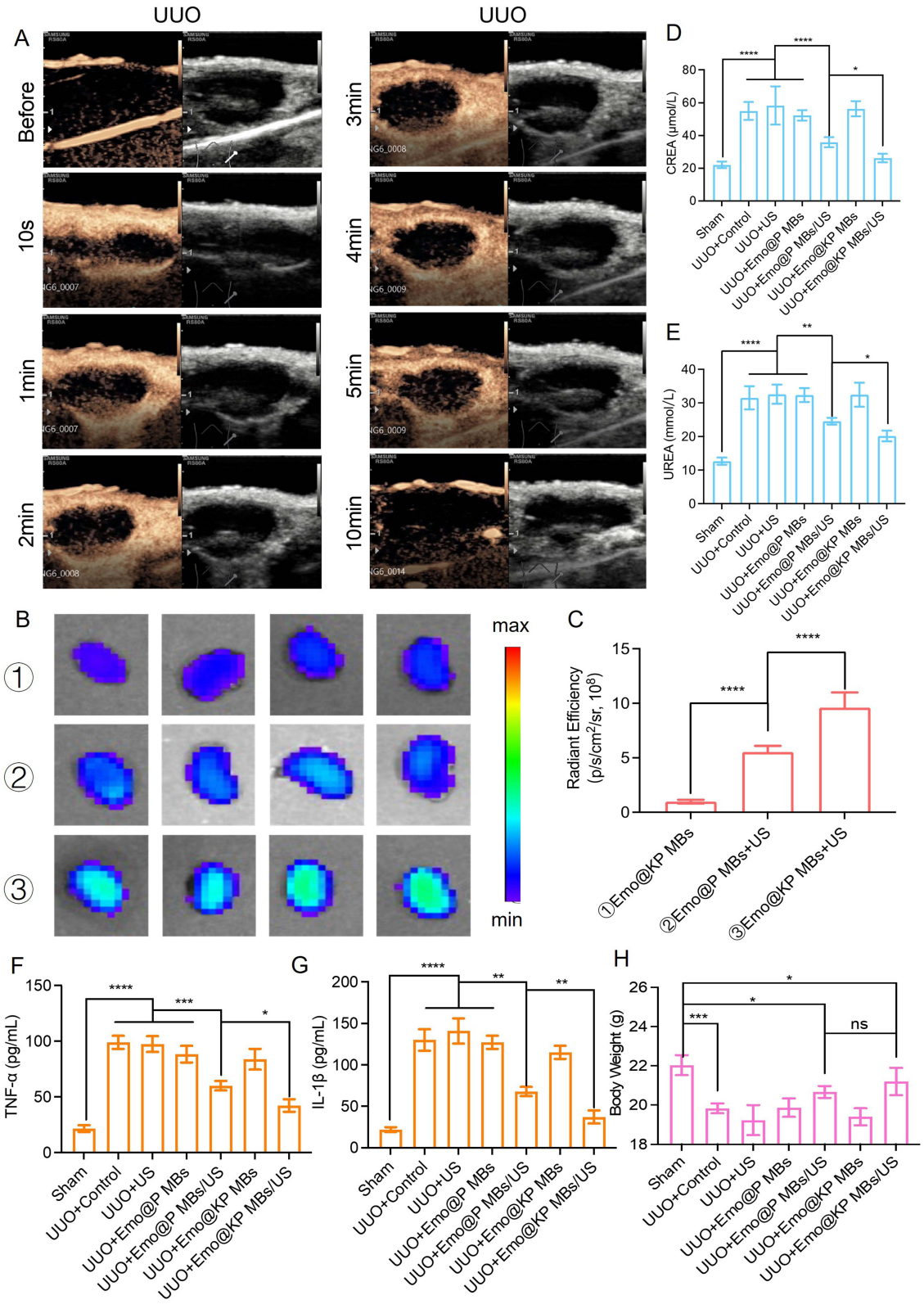

Figure 5 Contrast-enhanced ultrasound performance, distribution evaluation of the Emo@KP MBs in vivo and changes of blood indexes in mice after different treatments. (**A**) Evaluation of US imaging in vivo; (**B**) Fluorescence images of kidneys at 24 h after injection; (**C**) Semi-quantitative fluorescence intensity of (**B**); Blood CREA (**D**), UREA (**E**), TNF-α (**F**), IL-1β(**G**) and body weight (**H**) in mice after different treatments (* *P* < *0.05*, ** *P* < *0.01*, *** *P* < *0.001*, **** *P* < *0.0001*).

https://doi.org/10.2147/IJN.S499550

kidney area. The fluorescence signal of Emo@KP MBs + US group was the strongest among the three groups when the mice were killed at 24 hours after injection. In comparison to the Emo@KP MBs group, the fluorescence signal of the affected kidney in the Emo@KP MBs + US group was enhanced by approximately 9.86-fold. This enhancement was related to UTMD, which promoted the conversion of microbubbles into nanoparticles and facilitated the penetration of nanomaterials into tissues through the sonoporation effect and cavitation effect. The fluorescence signal of the affected kidney in the Emo@KP MBs + US group was enhanced by approximately 1.74-fold compared to the Emo@P MBs + US group (Figure 5B and C). This enhancement was related to the modification of αKIM-1 on the surface of the microbubbles. Following the conversion of Emo@KP MBs to Emo@KP NPs via UTMD, enhanced osmotic action enabled their entry into tissues, where they targeted the highly expressed KIM-1 in the affected kidney via αKIM-1, thereby increasing the tissue uptake. The above results indicated that Emo@KP MBs combined with US can significantly enhance drug accumulation in the diseased kidney, which may be related to the enhancement of vascular permeability and cell uptake by UTMD and the targeting effect of αKIM-1.

Changes in Blood Indexes

Compared with the Sham group, levels of CREA and UREA in UUO + Control group were increased, and the difference was statistically significant. This may be due to the fact that the compensatory reflex of the unblocked kidney is not sufficient to compensate for the dysfunction caused by the blocked kidney. Compared with UUO + Control group, CREA and UREA levels in UUO + Emo@P MBs/US and UUO + Emo@KP MBs/US groups were decreased, and the decrease was more significant in UUO + Emo@KP MBs/US group, which was not only due to the UTMD effect but also attributed to the specific targeting of αKIM-1 (Figure 5D and E).

Compared with the Sham group, the expression levels of inflammatory cytokines IL-1β and TNF-α in plasma of mice in UUO + Control group were significantly increased, but when Emo@P MBs and Emo@KP MBs were combined with US, the levels of inflammatory cytokines gradually normalized. And it is more significant in Emo@KP MBs/US, which should be also due to the specific targeting of αKIM-1 (Figure 5F and G).

Body weight is also an important indicator of health. After treatment, the weight of mice in each group was weighed, and the results showed that the weight of mice in UUO + Control group was lower than that in Sham group, and the weight of mice in UUO + US, UUO + Emo@P MBs and UUO + Emo@KP MBs groups were similar to that in UUO + Control group. These results indicated that there was almost no therapeutic effect in these groups, which further explained the stability of the prepared microbubbles. However, although the body weight of mice in UUO + Emo@P MBs/US and UUO + Emo@KP MBs/US groups was slightly lower than that in the Sham group, it was higher than that in UUO + Control group. These results indicated that microbubbles combined with ultrasound irradiation can relieve impaired kidney function, reduce inflammatory cell infiltration and improve the health status of mice (Figure 5H).

Pathological Staining of Diseased Kidney Tissue

HE staining was uniform in the renal tissue sections of the Sham group, and no abnormality was observed in morphology and structure. The renal tissue of UUO + Control group showed obvious mesangial matrix thickening, vacuolar degeneration of renal tubular epithelial cells, inflammatory cell infiltration and other pathological changes. The renal tissue lesions in UUO + US group were similar to those in UUO + Control group. The renal tissue lesions in UUO + Emo@P MBs group and UUO + Emo@KP MBs group were only slightly improved, indicating that the prepared drug-delivery microbubbles remained stable in blood circulation with little drug leakage. The renal tissue lesions in UUO + Emo@P MBs/US and UUO + Emo@KP MBs/US groups were significantly improved, indicating that UTMD can effectively promote micro to nano conversion and increase the permeability of vascular and tissue. The nanoparticles after blasted were more easily enter into the pathological tissue, and the improvement of UUO + Emo@KP MBs/US group was the best. These results indicated that the specific targeting of αKIM-1 increased the uptake of the drug by the diseased kidney (Figure 6A).

On Masson staining, a small amount of collagen was found in the glomeruli and interstitial of the kidney in the Sham group. Compared with the Sham group, the amount of collagen in the renal tissue of UUO + Control group was significantly increased, and the collagen distributed diffusely in the glomerular and interstitial regions of the kidney. The

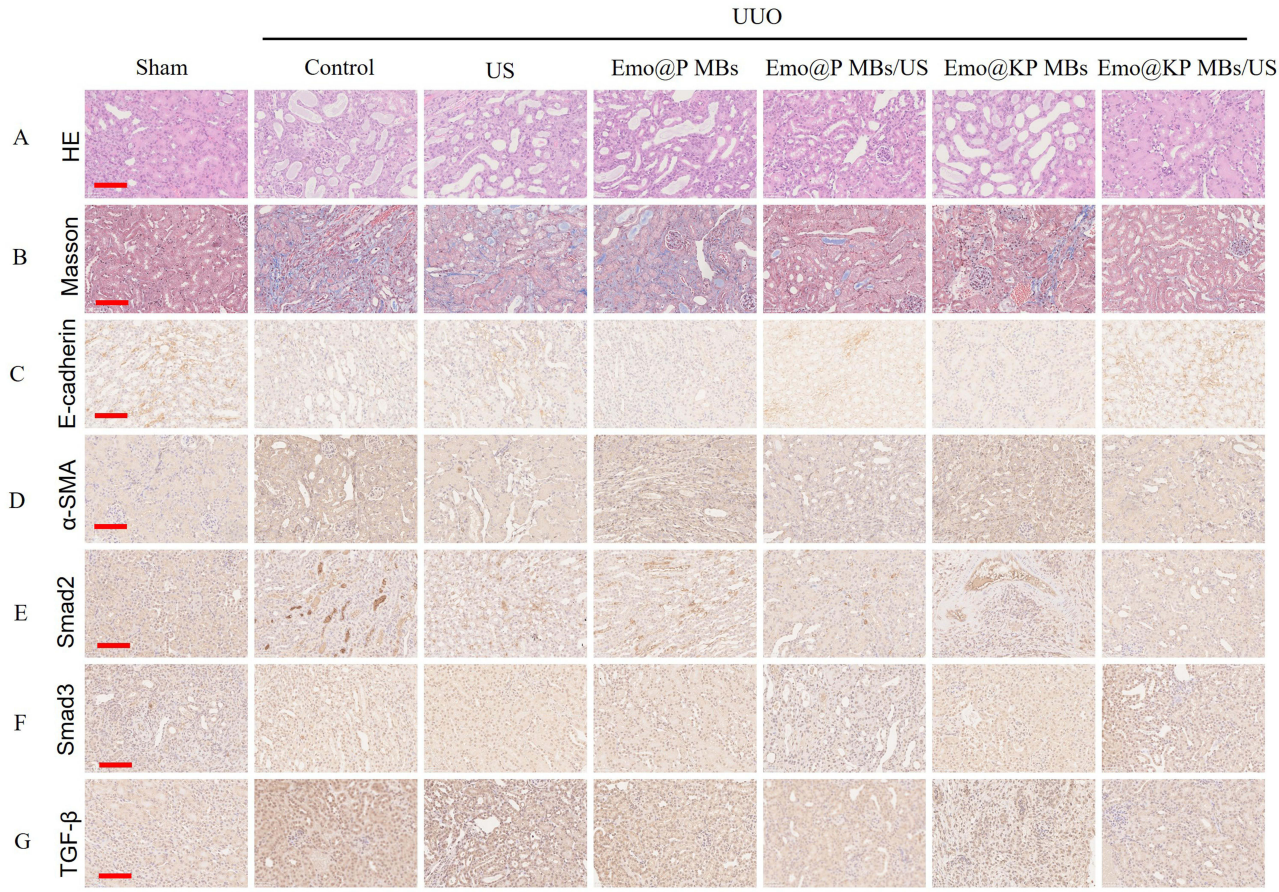

Figure 6 Pathological staining and immunohistochemical staining of kidneys in different treatment groups of mice. (**A**) HE staining of kidney sections from different treatment groups; (**B**) Masson staining of kidney sections from different treatment groups; (**C**–**G**). Expression of E-cadherin (**C**), α-SMA (**D**), Smad2 (**E**), Smad3 (**F**) and TGF-β (**G**) in kidney sections of mice in different treatment groups, Scale bar: 100 μm.

collagen in glomerular and renal interstitial area of mice in UUO + US, UUO + Emo@P MBs and UUO + Emo@KP MBs groups were similar to that in UUO + Control group, which further indicated the stability of the prepared microbubbles. The collagen content of renal tissue in UUO + Emo@ P MBs/US and UUO + Emo@KP MBs/US groups were significantly decreased, especially in UUO + Emo@KP MBs/US group, which could be attributed to the increased emodin release by UTMD and emodin uptake by αKIM-1 (Figure 6B).

Immunohistochemical Analysis of TGF-β/Smad Signaling Pathway

TGF-β can accelerate tissue fibrosis by regulating the transcriptional expression of extracellular matrix-related genes and plays a key role in the pathophysiological process of fibrotic diseases.[29] The development of renal fibrosis in response to any causative agent can be attributed to the secretion of excessive TGF-β1 by renal intrinsic cells, which activates the TGF-β1/Smad signaling pathway, induces phosphorylated Smads2/3 complexes to enter the nucleus of the cell, regulates the transcription of target genes, and activates ECM-producing cells such as myofibroblasts, accelerating the deposition of ECM. It is therefore considered that drugs which target the TGF-β1/Smad signaling pathway represent an effective form of treatment.

Previous studies[30] have demonstrated that Emodin can inhibit the activation of the TGF-β/Smad signaling pathway, reduce the expression of α-SMA protein, increase the expression of E-cadherin protein, inhibit the transformation of renal tubular epithelial mesenchyme, delay fibrosis of renal tissues, and exert a protective function on the kidney. In this study, Emodin was encapsulated into drug delivery carrier microbubbles and surface-modified with αKIM-1 antibody to form Emo@KP MBs. Theoretically, the Emo@KP MBs entry into UUO mice with diseased kidneys via the targeting of

https://doi.org/10.2147/IJN.S499550

αKIM-1, and its action by UTMD, can release Emodin, down-regulate TGF-β-induced phosphorylation of Smad2/3, thus reducing the up-regulation of αSMA and down-regulation of E-cadherin protein caused by obstruction. This, in turn, reduced the deposition of ECM and ameliorated the mesenchymal fibrosis in UUO mice.

Immunohistochemistry of renal tissues revealed a notable elevation in the expression of TGF-β, Smad2, Smad3, and α-SMA, accompanied by a pronounced decline in the expression of E-cadherin in the UUO group in comparison to the Sham group. These findings indicate that the TGF-β/Smad pathway is activated during the process of renal fibrosis subsequent to UUO. The TGF-β, Smad2, Smad3, α-SMA and E-cadherin in UUO + US group, UUO + Emo@P MBs and UUO + Emo@KP MBs group were similar to those in UUO + Control group, which further indicated the stability of the prepared microbubbles. In comparison to the UUO + Control group, the UUO + Emo@P MBs/US group demonstrated a downregulation of α-SMA, TGF-β, Smad2, and Smad3, accompanied by an upregulation of E-cadherin. This suggests that Emo@P MBs in the presence of UTMD may be capable of ameliorating the expression of RIF through the classical TGF-β1/Smad pathway. The UUO + Emo@KP MBs/US treatment resulted in a further decrease in the expression of α-SMA, TGF-β, Smad2, and Smad3, and a further increase in the expression of E-cadherin, which may be attributed to the targeting effect of αKIM-1 (Figure 6C–G).

Conclusion

RIF is a common pathological manifestation of CKD. EMT is thought to be the main cause of RIF. The UUO rodent experimental model of RIF is capable of inducing tubulointerstitial inflammation and fibrosis.[31] In our study, the results of blood biochemical experiments showed that impaired renal function in UUO mice resulted in increased CREA and UREA. Conversely, treatment with Emo@KP MBs/US significantly reduced the elevation of these markers. Histological examination by HE and Masson staining demonstrated that Emo@KP MBs/US treatment effectively improved the renal tissue structural abnormalities caused by RIF, alleviated renal tubule injury and collagen fiber deposition. Concomitantly, it was observed that Emo@KP MBs/US could decrease the expression of TGF-β1, Smad2/3, α-SMA and increase the expression of E-cadherin in EMT-related indicators in UUO mice. These results suggest that Emo@KP MBs/US can significantly improve renal fibrosis in mice, which can be attributed to αKIM-1 targeting and UTMD effect.

Acknowledgments

The authors gratefully acknowledge the financial support from Scientific and Technological Innovation Project of China Academy of Chinese Medical Sciences (CI2021A03309).

Disclosure

The authors report no conflicts of interest in this work.

References

1. Stevens S. Obstructive Kidney Disease. *Nurs Clin North Am*. 2018;53(4):569–578. doi:10.1016/j.cnur.2018.07.007
2. Martínez-Klimova E, Aparicio-Trejo OE, Tapia E, Pedraza-Chaverri J. Unilateral ureteral obstruction as a model to investigate fibrosis-attenuating treatments. *Biomolecules*. 2019;9(4):141. doi:10.3390/biom9040141
3. Wang Y, Chen L, Wang K, et al. Suppression of TRPM2 reduces renal fibrosis and inflammation through blocking TGF-β1-regulated JNK activation. *Biomed Pharmacother*. 2019;120:109556. doi:10.1016/j.biopha.2019.109556
4. Lee JH, Massagué J. TGF-β in developmental and fibrogenic EMTs. *Semi Cancer Biol*. 2022;86(Pt 2):136–145. doi:10.1016/j.semcancer.2022.09.004
5. Humphreys BD. Mechanisms of renal fibrosis. *Annu Rev Physiol*. 2018;80:309–326. doi:10.1146/annurev-physiol-022516-034227
6. Glanz V, Myasoedova VA, Sukhorukov V, et al. Transcriptional characteristics of activated macrophages. *Curr Pharm Des*. 2019;25(3):213–217. doi:10.2174/1381612825666190319120132
7. Sato Y, Yanagita M. Immune cells and inflammation in AKI to CKD progression. *Am J Physiol Renal Physiol*. 2018;315(6):F1501–F1512. doi:10.1152/ajprenal.00195.2018
8. Webster AC, Nagler EV, Morton RL, Masson P. Chronic kidney disease. *Lancet*. 2017;389(10075):1238–1252. doi:10.1016/S0140-6736(16)32064-5
9. Qi R, Yang C. Renal tubular epithelial cells: the neglected mediator of tubulointerstitial fibrosis after injury. *Cell Death Dis*. 2018;9(11):1126. doi:10.1038/s41419-018-1157-x
10. Iwano M. EMT and TGF-beta in renal fibrosis. *Front Biosci*. 2010;2(1):229–238. doi:10.2741/s60
11. Vega G, Alarcón S, San Martín R. The cellular and signalling alterations conducted by TGF-β contributing to renal fibrosis. *Cytokine*. 2016;88:115–125. doi:10.1016/j.cyto.2016.08.019

12. Hallan SI, Coresh J, Astor BC, et al. International comparison of the relationship of chronic kidney disease prevalence and ESRD risk. *J Am Soc Nephrol*. 2006;17(8):2275–2284. doi:10.1681/ASN.2005121273
13. Jha V, Garcia-Garcia G, Iseki K, et al. Chronic kidney disease: global dimension and perspectives. *Lancet*. 2013;382(9888):260–272. doi:10.1016/S0140-6736(13)60687-X
14. Imig JD, Khan MAH, Stavniichuk A, et al. Salt-sensitive hypertension after reversal of unilateral ureteral obstruction. *Biochem Pharmacol*. 2023;210:115438. doi:10.1016/j.bcp.2023.115438
15. Hung -C-C, Chen K-H, Hsu -H-H, et al. Noscapine alleviates unilateral ureteral obstruction-induced inflammation and fibrosis by regulating the TGFβ1/Smads signaling pathways. *Biochim Biophys Acta mol Cell Res*. 2024;1871(1):119594. doi:10.1016/j.bbamcr.2023.119594
16. Meng X-M, Nikolic-Paterson DJ, Lan HY. TGF-β: the master regulator of fibrosis. *Nat Rev Nephrol*. 2016;12(6):325–338. doi:10.1038/nrneph.2016.48
17. Xu H, Wu T, Huang L. Therapeutic and delivery strategies of phytoconstituents for renal fibrosis. *Adv Drug Deliv Rev*. 2021;177:113911. doi:10.1016/j.addr.2021.113911
18. Xiang Z, Sun H, Cai X, Chen D, Zheng X. The study on the material basis and the mechanism for anti-renal interstitial fibrosis efficacy of rhubarb through integration of metabonomics and network pharmacology. *Mol Biosyst*. 2015;11(4):1067–1078. doi:10.1039/C4MB00573B
19. Liu W, Gu R, Lou Y, et al. Emodin-induced autophagic cell death hinders epithelial-mesenchymal transition via regulation of BMP-7/TGF-β1 in renal fibrosis. *J Pharmacol Sci*. 2021;146(4):216–225. doi:10.1016/j.jphs.2021.03.009
20. Dou F, Liu Y, Liu L, et al. Aloe-Emodin ameliorates renal fibrosis via inhibiting PI3K/Akt/mTOR signaling pathway in vivo and in vitro. *Rejuvenation Res*. 2019;22(3):218–229. doi:10.1089/rej.2018.2104
21. Hu Q, Noor M, Wong YF, et al. In vitro anti-fibrotic activities of herbal compounds and herbs. *Nephrol Dial Transplant*. 2009;24(10):3033–3041. doi:10.1093/ndt/gfp245
22. Shukla V, Asthana S, Yadav S, Rajput VS, Tripathi A. Emodin inhibited NADPH-quinone reductase via competitive mode of inhibition and induced cytotoxicity in rat primary hepatocytes. *Toxicon*. 2020;S0041-0101(20):30422. doi:10.1016/j.toxicon.2020.10.018
23. Chen Y, Zhang T, Wu L, et al. Metabolism and toxicity of emodin: genome-wide association studies reveal hepatocyte nuclear factor 4α regulates UGT2B7 and emodin glucuronidation. *Chem Res Toxicol*. 2020;33(7):1798–1808. doi:10.1021/acs.chemrestox.0c00047
24. Yang L, Brooks CR, Xiao S, et al. KIM-1-mediated phagocytosis reduces acute injury to the kidney. *J Clin Invest*. 2015;125(4):1620–1636. doi:10.1172/JCI75417
25. Han WK, Bailly V, Abichandani R, Thadhani R, Bonventre JV. Kidney injury molecule-1 (KIM-1): a novel biomarker for human renal proximal tubule injury. *Kidney Int*. 2002;62(1):237–244. doi:10.1046/j.1523-1755.2002.00433.x
26. Yin W, Naini SM, Chen G, et al. Mammalian target of rapamycin mediates kidney injury molecule 1-dependent tubule injury in a Surrogate model. *J Am Soc Nephrol*. 2016;27(7):1943–1957. doi:10.1681/ASN.2015050500
27. Tang -T-T, Wang B, Li Z-L, et al. Kim-1 targeted extracellular vesicles: a new therapeutic platform for RNAi to treat AKI. *J Am Soc Nephrol*. 2021;32(10):2467–2483. doi:10.1681/ASN.2020111561
28. Song KH, Fan AC, Brlansky JT, et al. High efficiency molecular delivery with sequential low-energy sonoporation bursts. *Theranostics*. 2015;5(12):1419–1427. doi:10.7150/thno.13033
29. Budi EH, Schaub JR, Decaris M, Turner S, Derynck R. TGF-β as a driver of fibrosis: physiological roles and therapeutic opportunities. *J Pathol*. 2021;254(4):358–373. doi:10.1002/path.5680
30. Yang F, Deng L, Li J, et al. Emodin retarded renal fibrosis through regulating HGF and TGFβ-Smad signaling pathway. *Drug Des Devel Ther*. 2020;14:3567–3575. doi:10.2147/DDDT.S245847
31. Chevalier RL, Forbes MS, Thornhill BA. Ureteral obstruction as a model of renal interstitial fibrosis and obstructive nephropathy. *Kidney Int*. 2009;75(11):1145–1152. doi:10.1038/ki.2009.86